Study of ultraviolet-visible fluorescence emission following resonant Auger decay of the $2p^{-1}nl$ core-excited states of argon atoms

Tomasz J. Wasowicz[1]*, Antti Kivimäki[2,3], Matija Stupar[4], Marcello Coreno[5]

[1]*Department of Physics of Electronic Phenomena, Gdańsk University of Technology, ul. G. Narutowicza 11/12, 80-233 Gdańsk, Poland*

[2] *Nano and Molecular Systems Research Unit, University of Oulu, P.O. Box 3000, 90014 Oulu, Finland*

[3]*IOM-CNR, Laboratorio TASC, 34149 Trieste, Italy*

[4] *Laboratory of Quantum Optics, University of Nova Gorica, Nova Gorica, Slovenia*

[5] *ISM-CNR, LD2 Unit Basovizza Area Science Park, 34149 Trieste, Italy*

Keywords: photon-photon delayed-coincidence technique, argon, Ar 2*p* excitation, core-excited states, Auger decay

*Corresponding author: tomasz.wasowicz1@pg.edu.pl; twasowicz@mif.pg.gda.pl

PACS: 29.20.Lq; 29.30.−h; 32.30.-r; 32.30.Jc; 34.50.Fa; 78.70.En

Abstract

We have studied the excitation and relaxation of Ar^+ ions populated in resonant Auger decay from the Ar $2p^{-1}nl$ core-excited states by using ultraviolet-visible fluorescence spectroscopy and photon-photon delayed coincidence technique. Fluorescence emission yields were measured in the photon energy range of 240-255 eV for the $3s^23p^4(^1D)5s(^2D) \rightarrow 3s^23p^4(^1D)4p(^2F)$ (393 nm) and $3s^23p^4(^1D)4d(^2F) \rightarrow 3s^23p^4(^1D)4p(^2F)$ (335 nm) transitions as well as for the 380-500 nm wideband emission. Delayed coincidence photon decay curves for the cascade transitions of the 335/459 nm and 393/459 nm lines were measured at the four most intense Ar 2*p* core excitations and the coincidence yields for both studied cascade channels were obtained at these Ar 2*p* excitations.

1. Introduction

Investigations of excitation and relaxation of the core-excited states of atoms and molecules are motivated by the interest to unravel the role played by the electron-electron correlation, contributing to the development of modern atomic theory [1]. Besides the fundamental knowledge, the spectroscopy of highly excited states has many applications, including the modeling of laboratory plasmas, design of fusion reactors and finding out the chemical composition of astronomical objects [1]. Core-excited states are built by the selective excitation of an inner-shell electron to an unoccupied (Rydberg) orbital. They decay predominantly via resonant spectator Auger transitions, where an outer electron fills the core hole and another is ejected. During the decay, the excited electron can stay in the same orbital or shake up or down to another orbital [2]. The core-excited states of Ar have been most extensively studied for the excitations of the *2p* electrons into the *ns* and *nd* Rydberg orbitals. They appear as distinct peaks below the $2p^{-1}(^2P_{3/2,1/2})$ ionization thresholds in photoabsorption [3], electron energy-loss spectra [4] and photoionization [5] spectra. The argon $2p^{-1}nl$ states decaying via resonant Auger transitions mostly populate valence-excited $3s^23p^4nl$, $3s^13p^5nl$ and $3s^03p^6nl$ states of the Ar^+ ions. The resonant Auger spectra of argon have been studied using electron spectroscopy [6]-[8] and electron–electron coincidence spectroscopy [9],[10]. The excited Ar^+ ions further decay to lower excited states by emission of the ultraviolet-visible (UV-VIS) fluorescence [11]-[14] or directly to the ground ionic state by UV emission [15],[16]. Samson and coworkers [12], [17] suggested that the excited ionic states of argon may be formed directly in the resonant Auger decay of the Ar 2*p* hole states or indirectly via radiative cascades. In this perspective, Flesch et al [13] have performed the most extensive UV-VIS fluorescence studies in the Ar 2*p* core-excitation region. The fluorescence spectra of argon covering the wavelength range of 300-500 nm measured at the Ar $2p_{1/2} \rightarrow 3d$, $2p_{3/2} \rightarrow 3d$ and $2p_{3/2} \rightarrow 4s$ resonances revealed a number of transitions in Ar^+, which arise from the above-mentioned direct and indirect mechanisms [13]. For example, the resonant Auger decay

directly populates the states of the $3s^2 3p^4(^1D)4d(^2F)$ and $3s^2 3p^4(^1D)5s(^2D)$ terms, which increases the intensity of the 335 and 393 nm emission lines, respectively, when these states radiatively decay to the intermediate $3s^2 3p^4(^1D)4p(^2F)$ term (see Figure 1). The latter term de-excites in the cascading decay to the $3s^2 3p^4(^1D)4s(^2D)$ term, yielding a stronger 459 nm fluorescence line. The cascade transitions hampered the analysis of the fluorescence spectra and time-resolved dispersed fluorescence measurements had to be applied to distinguish between the two decay modes [13].

In the context presented above, the photon-photon coincidence technique allows one to investigate cascade effects and provides more insight into the dynamics of the discussed processes. In this paper, we present the fluorescence studies of photoexcitation and decay of the $2p^{-1}nl$ core-excited states of Ar atoms using the photon-induced fluorescence technique combined with a photon-photon delayed-coincidence detection system. In particular, we have used the photon induced fluorescence technique to measure the fluorescence yield spectra of the $3s^2 3p^4(^1\mathrm{D})5s(^2\mathrm{D}) \rightarrow 3s^2 3p^4(^1\mathrm{D})4p(^2\mathrm{F})$ (393 nm) and $3s^2 3p^4(^1\mathrm{D})4d(^2\mathrm{F}) \rightarrow 3s^2 3p^4(^1\mathrm{D})4p(^2\mathrm{F})$ (335 nm) emission lines over the energy range of the Ar 2p excitations (240-255 eV). We have also utilized the photon-photon delayed-coincidence system in order to observe events where the decay of the 2*p* inner shell excited argon in the 240-255 eV energy range leads to the emission of two UV/visible photons. The coincidence measurements have been performed for the 335/459 nm (channel 1) and 393/459 nm (channel 2) emission cascades (shown in Figure 1) at various photon energies across the Ar 2*p* excitations. For those cascade transitions the delayed coincidence photon decay curves have been measured over the energy range of excitation of the $2p^{-1}nl$ states of argon. The coincidence yields have been determined from the obtained curves.

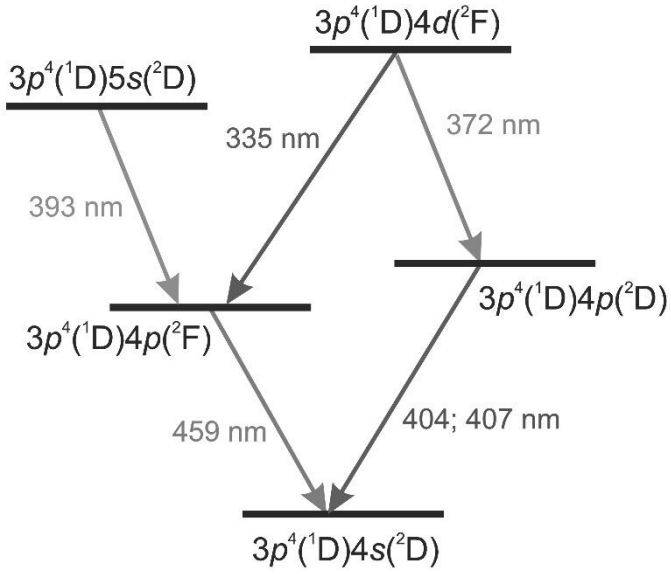

Figure 1. Schematic diagram of fluorescence cascade transitions occurring in Ar^+ ions after the excitation of 2*p* electrons to empty orbitals.

2. Experiment

The experiments were performed at the low-energy branch of the Gas Phase Photoemission beamline at the Elettra synchrotron radiation facility in Trieste, Italy. The branch line can be used in the photon energy range of 14-280 eV. A spherical grating monochromator equipped with five interchangeable gratings can provide high resolving power (>10^4) throughout the operating range. In the present measurements, the slits of the monochromator were optimized in order to increase count rates, but without deteriorating too much the photon resolution. As a consequence, the photon resolution was still high enough to resolve the Ar $2p_{1/2} \rightarrow 4s$ and Ar $2p_{3/2} \rightarrow 3d$ resonances.

In the measurements, the photon-induced fluorescence technique [18]-[22] combined with a photon-photon delayed-coincidence detection system has been applied. Figure 2 shows the top view of the used experimental set-up for photon-induced fluorescence spectroscopy (PIFS). An effusive jet of Ar gas was introduced through a needle in the interaction region where it was crossed by the monochromatic photon beam coming from the beamline. The

partial pressure of Ar in the interaction region was estimated to be about 1000 times higher than that of the rest gas, hence fluorescence from rest-gas molecules is considered negligible. A spherical mirror collected light that was emitted along the electrical vector of the linearly polarized incident light and collimated it, after which the light exited the vacuum chamber through a quartz window. For the purposes of these studies, a dedicated fluorescence detection system was designed and constructed at Gdańsk University of Technology and transferred to the Gas Phase beamline at Elettra. It consisted of a beam splitter and two optical channels, each incorporating interference or wideband filters followed by a photomultiplier tube. Outside the vacuum chamber, this system allowed us to divide the fluorescence signal into two parts with the aid of a beam splitter (50T/50R), which was selected according to the wavelength range of the studied emission. The transmitted part of the light beam was filtered with an Edmonds narrow-band interference filter (e.g. 337±5 nm, 392±5 nm) before it was detected by the PMT 1 tube, model 9828WB from ET Enterprises, whose full operation range is 200-800 nm. The reflected part of the split beam went through a color filter before being detected by a Hamamatsu R6095 photomultiplier tube (PMT 2). A filter with the band pass 380-500 nm was most often used in this arm of the experiment. Moreover, the total ion yield (TIY) was simultaneously measured utilizing a microsphere plate detector that was operated in current mode. The photodiode at the exit of the vacuum chamber monitored the photon flux for normalization purposes.

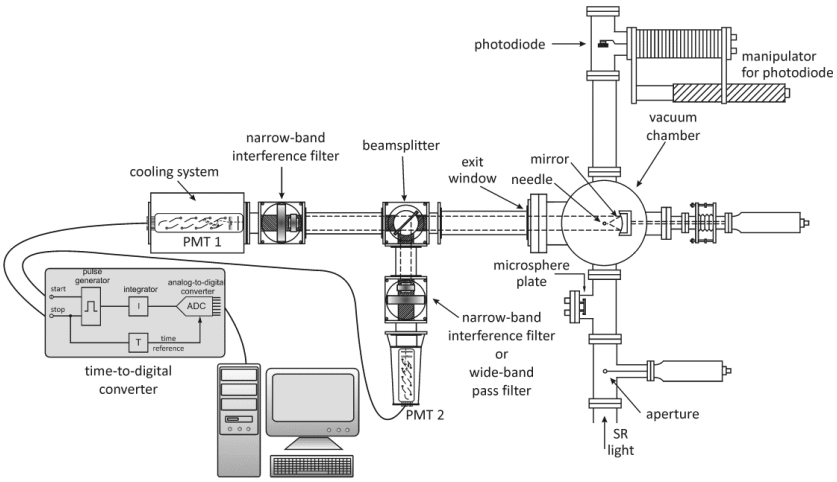

Figure 2. Scheme of the experimental set-up.

The experiments were carried out in the multi-bunch operation of the storage ring, hence incident photons arrived every 2 ns in the interaction region. We mostly used a continuous data collection mode, in which a pulse generator (Stanford Research DG535) gave start pulses with the frequency of 10 Hz and the signals from the two PMTs, after going through signal processing electronics (preamplifier, pulse discriminators, NIM->TTL conversion), provided stop signals in two separate channels (STOP1 and STOP2). The start and stop signals were fed into a time-to-digital converter system (ATMD-GPX from Acam Messelectronic GmBH), whose time resolution is 80 ps. The collection window remained open for 80 ms after each start signal, followed by 20 ms for writing the tag of the start pulse and the arrival times of stop signals in an array form in a data file. Coincidences between the STOP1 and STOP2 signals were searched for after the completion of the measurement by using a self-written procedure in the data analysis program Igor. The procedure searched for STOP1 and STOP2 signals whose arrival times were separated by less than a selectable maximum time difference and saved that arrival time difference as a good data point, while arrival time differences larger than the maximum time difference were discarded. The procedure allowed either STOP1 or STOP2 signal to be detected first. After processing all

data arrays of a given measurement in that way, the procedure made histograms of the data points by binning saved acceptable arrival time differences within chosen time steps (e.g. 5 ns). Peaks appearing in these histograms may indicate coincidences between two photons detected with the two PMTs, while accidental coincidences form a background that can extend over all values of arrival time differences.

3. Results and discussion

3.1 Total ion yield and undispersed fluorescence yield

At first, the emission yield of undispersed fluorescence was measured in the wavelength range of 380-500 nm. We call it the violet-blue fluorescence yield and present it in Fig. 3a as a function of photon energy in comparison with the total ion yield (Fig. 3b). Both curves show resonances corresponding to the excitations to the $2p^{-1}nl$ (n = 3, 4, 5; l = s, d) Rydberg states. The energy positions of those Rydberg states and Ar 2p ionization energies are indicated by vertical bars. The assignments of the Rydberg states and the ionization thresholds located at 248.628 eV (Ar $2p_{3/2}^{-1}$) and 250.776 eV (Ar $2p_{1/2}^{-1}$) were taken from [4]. In the energy range from 248 eV up to about 252 eV, the maxima in the total ion yield are superimposed on a steady rising background, which may mostly be ascribed to the 2p ionization continuum [14]. The total ion yield is mostly caused by Ar^+ ions, with minor contributions from Ar^{2+} and more highly charged Ar ions [5].

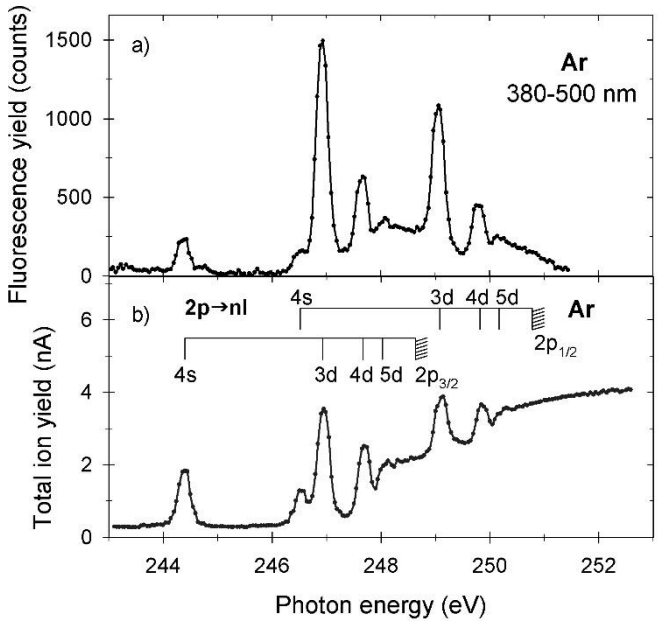

Figure 3. a) The undispersed fluorescence yield in the wavelength range 380-500 nm; b) the total ion yield at the Ar 2*p* edge. The spectra were normalized to the photon flux. The energy positions of the core-to-Rydberg states and Ar 2*p* ionization energies are indicated by vertical bars.

As seen in Fig. 3 the violet-blue fluorescence yield resembles the total ion yield. This is because numerous radiative transitions occurring in this spectral regime follow the resonant Auger decay of core-excited states [13]. But in contrast to the total ion yield, the violet-blue fluorescence yield does not show an increasing background above the Ar 2p ionization limits. Since the predominant decay channel in the 2p ionization continuum is normal Auger decay, which produces Ar^{2+} ions, this observation may indicate that Ar^{+} is the major source of fluorescence emission at the Ar 2*p* edge [5], [13]. Indeed, the $3s^2 3p^4\ nl$ states of Ar^{+} [6],[7] can further decay via the emission of fluorescence light in the UV-VIS regime [13],[14]. The present violet-blue fluorescence yield reveals strong intensities at the $2p^{-1}3d$ and $2p^{-1}4d$ excitations. This is in agreement with the work of de Gouw et al. [6] who showed that the shake-up processes play a dominant role in the resonant Auger decay of the $2p_{3/2}{}^{-1}3d$ and

$2p_{3/2}^{-1}4d$ states, populating the $3s^2 3p^4 4d$ (or 5*d*, 6*d*) final states that can further decay by emitting UV-VIS light. A notable difference between the total ion yield and violet-blue fluorescence yield is that the fluorescence emission at the $2p^{-1}4s$ excitation is much lower. This is because the $2p^{-1}4s$ state decays predominantly via spectator Auger processes in which the excited electron stays in the same orbital [6]. The resulting $3s^2 3p^4 4s$ final states emit fluorescence light at UV wavelengths not covered by the present detection system. The fluorescence seen at 244.4 eV should arise due to emission following shake-up processes. The probability to populate the $3s^2 3p^4(^3P)5s$ state via shake-up transitions at the $2p^{-1}4s$ resonance was estimated to be 11% [6]. This state may further decay via cascade transitions in the visible regime.

It is of note that fluorescence decay could, in principle, take place after normal Auger decay (i.e. from Ar^{2+}) because the Auger spectrum contains so-called correlation satellites that involve the occupation of 3*d*, 4*d*, 4*s*, … orbitals in the final state [23]. These final states have electron configurations of type $3p^3 nl^1$, where *nl* = 4*s*, 3*d*, 5*s*, 4*d*, …, and they are an integral part of the normal Auger spectrum. In particular, the correlation satellites are populated straight away when the photon energy exceeds the Ar 2*p* ionization limits. If fluorescence emission followed correlation satellite transitions of normal Auger decay, the violet-blue fluorescence yield in Fig. 3(a) would remain non-zero in the Ar 2*p* ionization continuum. Our experiment shows that the fluorescence yield tends to zero when photon energy (or excess energy, *hν*–IP(Ar 2*p*)) grows.

3.2 Dispersed fluorescence excitation spectra

For purposes of this study, the λ=335 nm and λ=393 nm lines have been selected because i) they are well separated, which is important when using interference filters, ii) they occur in wavelength ranges, which allow the observation of state-selective excitations and iii) these transitions feed the $3s^2 3p^4(^1D)4p(^2F)$ term, which can further relax via transitions (459 nm) to

the $3s^2 3p^4(^1\mathrm{D})4s(^2\mathrm{D})$ term, allowing the study of two different cascade channels after the Ar $2p$ excitations. Therefore in the next step, the fluorescence excitation spectra of these selected lines were measured. These curves are displayed in Fig. 4.

The 337 nm narrow-band interference filter transmitted light in the 337±5 nm wavelength range. In this wavelength range only the $3s^2 3p^4(^3\mathrm{P})4d(^2\mathrm{P}_{3/2}) \rightarrow 3s^2 3p^4(^3\mathrm{P})4p(^2\mathrm{S}_{1/2})$ (338.85 nm) and $3s^2 3p^4(^1\mathrm{D})4d(^2\mathrm{F}) \rightarrow 3s^2 3p^4(^1\mathrm{D})4p(^2\mathrm{F})$ (335 nm) transitions have high enough transition probabilities [24]-[26] to be detected in the present experiment. The emission from the $3s^2 3p^4(^3\mathrm{P})4d(^2\mathrm{P}_{3/2})$ state can be excluded from the analysis considering that after $2p$ excitations the transition rate to the $3s^2 3p^4(^3\mathrm{P})4d(^2\mathrm{P}_{3/2})$ state is an order of magnitude lower than to the states of the $3s^2 3p^4(^1\mathrm{D})4d(^2\mathrm{F})$ term [7]. This is in agreement with the studies of Flesch *et al.* who observed in their dispersed fluorescence spectra (Fig. 1 of [13]) a very narrow line centered at 335 nm and no emission at ~339 nm. The $4d(^2\mathrm{F})$ term consists of the $4d(^2\mathrm{F}_{5/2})$ and $4d(^2\mathrm{F}_{7/2})$ states that in the wavelength range considered emit photons only via transitions into the $4p(^2\mathrm{F}_{5/2})$ and $4p(^2\mathrm{F}_{7/2})$ states of the $3s^2 3p^4(^1\mathrm{D})4p(^2\mathrm{F})$ term [24]. Mursu *et al.* [7] established that only the $4d(^2\mathrm{F}_{5/2})$ state is populated directly in the resonant Auger process. They showed that the J=5/2 component appears at the $2p_{1/2}^{-1}3d$ excitation, whereas the J=7/2 component is not observed [7]. Thus, the multiplet consists of two components: $4d(^2\mathrm{F}_{5/2}) \rightarrow 4p(^2\mathrm{F}_{5/2})$ (λ=335.09 nm) and $4d(^2\mathrm{F}_{5/2}) \rightarrow 4p(^2\mathrm{F}_{7/2})$ (λ=336.55 nm). However, the probability of the $4d(^2\mathrm{F}_{5/2}) \rightarrow 4p(^2\mathrm{F}_{7/2})$ transition is an order of magnitude lower than that of the $4d(^2\mathrm{F}_{5/2}) \rightarrow 4p(^2\mathrm{F}_{5/2})$ transition [24]-[26]. Therefore, the emission measured with the 337 nm filter arises most likely from the $3s^2 3p^4(^1\mathrm{D})4d(^2\mathrm{F}_{5/2}) \rightarrow 3s^2 3p^4(^1\mathrm{D})4p(^2\mathrm{F}_{5/2})$ transition. The corresponding fluorescence excitation spectrum of Ar^+ excited to the $3s^2 3p^4(^1\mathrm{D})4d(^2\mathrm{F})$ term is shown in Fig. 4a.

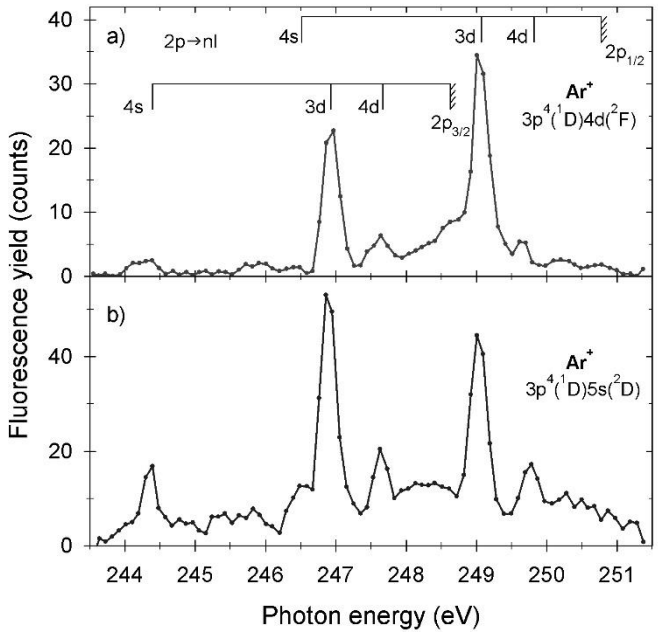

Figure 4. Fluorescence excitation spectra at the Ar 2*p* edge. The spectra were normalized to the photon flux. The energy positions of the core-to-Rydberg resonances and Ar 2*p* ionization energies are indicated by vertical bars.

The yield measured with the 337 nm interference filter displays a state-selective pattern (Fig. 4a). It shows strong peaks due to the $2p_{1/2}^{-1}3d$ and $2p_{3/2}^{-1}3d$ resonances, but compared to the violet-blue fluorescence yield and total ion yield, their intensities are inverted. Previously, this yield was reported at the Ar 2*p* edge by Flesch and coworkers [13]. However, a more detailed discussion of the spectral features is possible, thanks to the improved photon energy resolution of the present experiment. It is expected [7] that the $3s^23p^4(^1\mathrm{D})4d(^2\mathrm{F}_{5/2})$ state should be only populated at the $2p_{3/2}^{-1}4d$ and $2p_{1/2}^{-1}3d$ excitations. However, the $2p_{3/2}^{-1}4d$ excitation was not recorded in the previous fluorescence yield [13], whereas the emission occurring from the $2p_{3/2}^{-1}3d$ resonance was observed. In contrast, our fluorescence spectrum shows clear optical emission occurring from all of those resonances. Moreover, the $2p_{3/2}^{-1}4s$ resonance is visible in our spectrum. The weak population of the $3s^23p^4(^1\mathrm{D})4d$ final states in resonant Auger decay at the $2p_{3/2}^{-1}4d$ resonance would let us expect a low fluorescence

intensity [6], [7]. However, the fluorescence emission may become enhanced through cascade processes induced by shake-up transitions in resonant Auger decay. For instance, the $3s^2 3p^4(^1\mathrm{D})5\mathrm{d},6d$ shake-up final states have higher intensities than the spectator final states in the resonant Auger spectrum and they could decay as follows: $3s^2 3p^4(^1\mathrm{D})5\mathrm{d},6d \rightarrow 3s^2 3p^4(^1\mathrm{D})5\mathrm{p},6p \rightarrow 3s^2 3p^4(^1\mathrm{D})4d$. Inasmuch the emission occurring at the $2p_{3/2}^{-1}4s$ resonance is surprising, because the Auger resonance spectra [6], [7] indicated that the $3s^2 3p^4(^1\mathrm{D})4d(^2\mathrm{F})$ term is not populated upon this excitation.

The other narrow-band interference filter (392 nm) used in the experiment covered the wavelength range of 392±5 nm. Only the $3s^2 3p^4(^3\mathrm{P})4d(^4\mathrm{P}_{3/2})$ and $3s^2 3p^4(^1\mathrm{D})5s(^2\mathrm{D}_{3/2;5/2})$ states populated after the Ar $2p$ excitations [6], [7] decay via the emission of fluorescence in this wavelength range [24]. Intense Ar^+ lines are identified in emission spectroscopy at 393.25 nm, corresponding to the transition $3s^2 3p^4(^3\mathrm{P})4d(^4\mathrm{P}_{3/2}) \rightarrow 3s^2 3p^4(^3\mathrm{P})4p(^4\mathrm{S}_{3/2})$, and between 392.57 and 394.61 nm due to the $3s^2 3p^4(^1\mathrm{D})5s(^2\mathrm{D}) \rightarrow 3s^2 3p^4(^1\mathrm{D})4p(^2\mathrm{F})$ transitions [24]. This finding is in agreement with the UV-VIS spectra of Flesch *et al.* [13] that show a well separated feature at 393±2 nm. However, a contribution from the close-lying Ar^+ emission line at λ=393.25 nm to the 393 nm fluorescence can be ruled out since the $4d(^4\mathrm{P}_{3/2})$ state is only populated upon the $2p_{1/2}^{-1}3d$ excitation [6], [7]. The emission yield shown in Fig. 4b indicates instead that this decay channel is induced by several Ar $2p$ excitations. Only the $3s^2 3p^4(^1\mathrm{D})5s(^2\mathrm{D})$ term can be populated at several Ar $2p$ excitations [6], [7]. Mursu *et al.* [7] established that the J=5/2 component of the $3s^2 3p^4(^1\mathrm{D})5s(^2\mathrm{D})$ term is populated directly in the Auger process, whereas the J=3/2 component is not observed. Taking this into account and keeping in mind that the $3s^2 3p^4(^1\mathrm{D})5s(^2\mathrm{D}_{5/2}) \rightarrow 3s^2 3p^4(^1\mathrm{D})4p(^2\mathrm{F}_{7/2})$ transition has the transition probability more than one order of magnitude higher than the $3s^2 3p^4(^1\mathrm{D})5s(^2\mathrm{D}_{5/2}) \rightarrow 3s^2 3p^4(^1\mathrm{D})4p(^2\mathrm{F}_{5/2})$ transition [24], we assign the fluorescence occurring at 393 nm to the $3s^2 3p^4(^1\mathrm{D})5s(^2\mathrm{D}_{5/2}) \rightarrow 3s^2 3p^4(^1\mathrm{D})4p(^2\mathrm{F}_{7/2})$ transition. The corresponding fluorescence yield is shown in Fig. 4b. To the best of our knowledge it has not been reported earlier. Previously,

Flesch and coworkers [13] tentatively attributed its production to the strongest $2p_{1/2}^{-1}3d$, $2p_{3/2}^{-1}3d$ and $2p_{3/2}^{-1}4s$ resonances on the basis of three fluorescence spectra measured at the corresponding energies. The present yield clearly shows the highest intensities at these resonances. Moreover, it displays well separated structures due to the $2p_{1/2}^{-1}4d$ and $2p_{3/2}^{-1}4d$ excitations and even reveals the $2p_{1/2}^{-1}4s$ resonance at 246.5 eV. These findings are in good agreement with the resonant Auger spectra [7], where it was shown that the $3s^23p^4(^1D)5s(^2D_{5/2})$ final state is populated with similar intensities at the $2p^{-1}4s$ and $2p^{-1}3d$ excitations. The $3s^23p^4(^1D)5s(^2D_{5/2})$ state is also reached in the decay of the $2p^{-1}4d$ core-excited states [7].

3.3 Photon-photon coincidences

By observing delayed coincidences between the initiating photons (335 or 393 nm**)** and the subsequent decay photons (459 nm), a time spectrum is obtained. Thus in the next step, we have measured coincidences for the 335/459 nm and 393/459 nm photon combinations (a scheme of transitions is shown in Figure 1) at various photon energies below the Ar 2*p* ionization potential. The coincidences for the first cascade (335/459 nm) were not intense and required long acquisition times (~12 h). Thus due to time constraints they were only measured at the most intense excitations corresponding to the $2p_{3/2} \rightarrow 3d$ and $2p_{1/2} \rightarrow 3d$ resonances. The coincidences for channel 2 (393/459 nm) were stronger and we measured them at the $2p_{3/2} \rightarrow 4s$, $2p_{3/2} \rightarrow 3d$, $2p_{3/2} \rightarrow 4d$ and $2p_{1/2} \rightarrow 3d$ resonances.

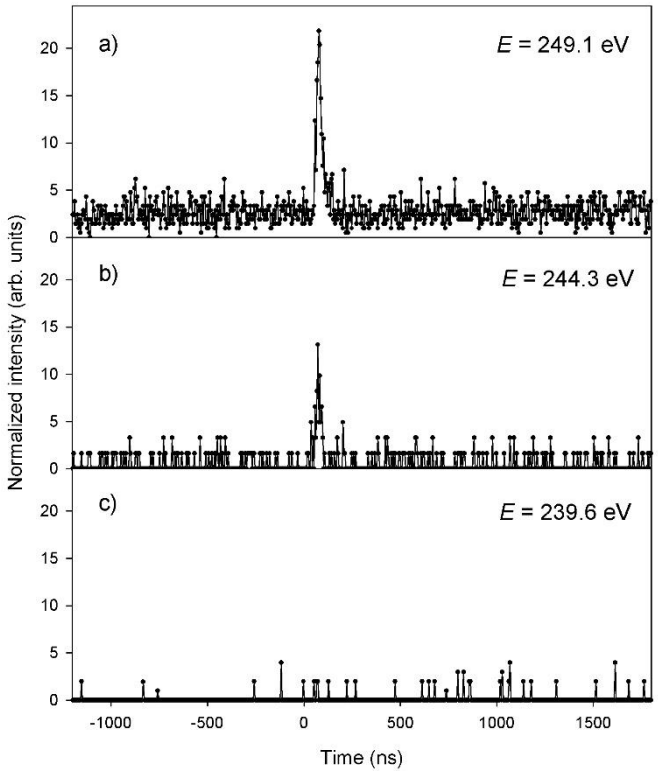

Figure 5. Delayed coincidence photon decay curves measured between the 393 and 459 nm photons a) at the Ar $2p_{1/2} \rightarrow 3d$ resonance (249.1 eV) b) at the Ar $2p_{3/2} \rightarrow 4s$ resonance (244.3 eV), and c) below the first Ar $2p$ resonance at 239.6 eV. The intensity scale in the panels results from binning arrival times in 5 ns wide windows.

Fig. 5 shows delayed coincidence photon decay curves (black dots) between the 393 and 459 nm photons. At the resonances (Fig. 5a and 5b) a reasonable signal-to-noise ratios were obtained and thus coincidences measured at the corresponding energies are clearly seen superimposed on a background of the accidental coincidences between uncorrelated events. Fig. 5c shows no coincidence signal.

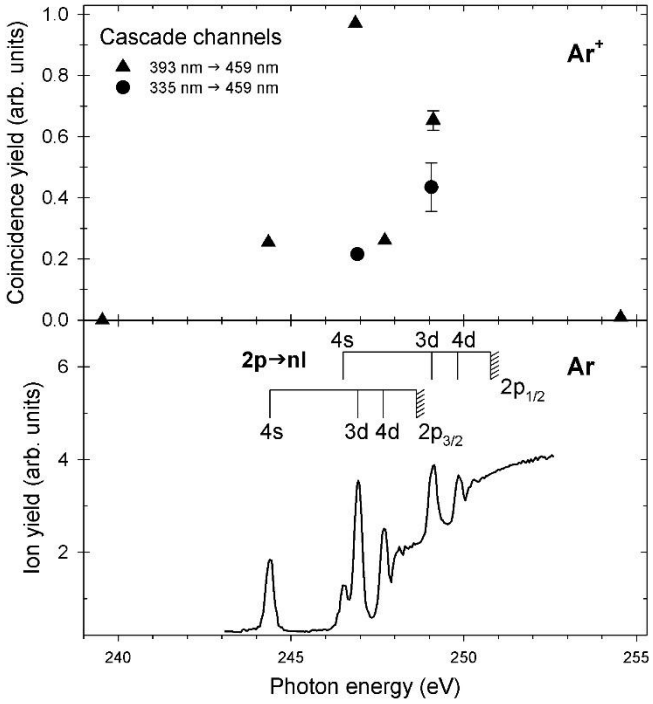

Figure 6. Coincidence yields as a function of photon energy for both studied cascade channels. The total ion yield is presented in the lower panel for comparison.

The coincidence yields were next obtained by integrating over the area of each coincidence photon decay curve. The background due to accidental coincidences was taken to be the average of that below and above the studied coincidence band and was subtracted from the spectra. The resulting coincidence yields were normalized to the Ar pressure (mbar), photon flux (μA) and recording time (min). In Fig. 6 we present the coincidence yields as a function of photon energy for both studied cascade channels. To be clear to which resonances the experimental points refer we also show the total ion yield in the lower panel. The obtained coincidence yields show a strong dependence on the excitation energy. The relative coincidence intensities of each photon combination resemble the intensities of the resonances in the corresponding fluorescence yields (shown in Fig. 4a and 4b) and demonstrate that each transition can selectively populate the $3s^2 3p^4(^1\mathrm{D})4p(^2\mathrm{F})$ intermediate term. It is of note that fluorescence usually exhibits anisotropic angular distribution according to the transition that

may affect the fluorescence yields and in consequence the photon-photon coincidence yields as well [27]. Such an influence can be corrected by obtaining the anisotropy parameter (see eg. [28]), which, however, was outside the scope of the present work.

For the 393/459 nm photon combination we have additionally measured the coincidences below the first Ar 2*p* resonance at 239.6 eV and above the ionization limits at 254.6 eV, where in fluorescence yield no traces of pre-edge and the post-collision processes, respectively, are expected. Both results are presented in Fig. 6. No coincidence signal was recorded at those energies (see Fig. 5c). This observation in connection with the apparent coincidences measured for the Ar 2*p* resonances represents direct evidence that Ar^+ is the source of radiative relaxation at the Ar 2*p* edge.

Summary

We have investigated photoexcitation and relaxation of atomic argon in the 240-255 eV photon energy range (the Ar 2*p* edge) using photon-induced fluorescence technique combined with the photon-photon delayed-coincidence detection system. We have recorded the fluorescence excitation spectra of the $3s^2 3p^4(^1\mathrm{D})5s(^2\mathrm{D}_{5/2}) \rightarrow 3s^2 3p^4(^1\mathrm{D})4p(^2\mathrm{F}_{7/2})$ (393 nm), $3s^2 3p^4(^1\mathrm{D})4d(^2\mathrm{F}_{5/2}) \rightarrow 3s^2 3p^4(^1\mathrm{D})4p(^2\mathrm{F}_{5/2})$ (335 nm) transitions and of 380-500 nm wideband emission as well as delayed coincidence photon decay curves for the 335/459 nm and 393/459 nm emission cascades. This allowed determination of the coincidence yields. The comparison with the measured total ion yield shows that the fluorescence yields are endowed with the different, state-selective patterns. The coincidence measurements performed for the 335/459 nm and 393/459 nm photon cascades at the four most intense Ar 2*p* resonances demonstrate that this state-selective behavior of initial excitation is further forwarded through radiative transition into the lower $3s^2 3p^4(^1\mathrm{D})4p(^2\mathrm{F}_{7/2,5/2})$ states. Indeed, the coincidence yields of each photon combination resemble the intensities of the resonances at the corresponding

fluorescence yields. Moreover, our results clearly show that Ar^+ is the source of radiative relaxation at the Ar 2*p* edge.

The present photon-photon coincidence technique could be used for any samples. However, it is most suitable to the studies of emission from atoms or atomic fragments, where intensity is concentrated on narrow emission lines. Cascade transitions in atoms, studied in the present paper, can be expected to be common after resonant Auger decay and they can destroy the population and polarization of the initial states of the measured optical transitions [29], [30]. Measuring cascade photons in coincidence would help to unravel their contribution to the studied transitions. The present technique could also be used to detect dissociation channels where two excited fragments are produced simultaneously in molecular dissociation. Such a channel has been observed in the doubly excited states of the water molecule: $H_2O \rightarrow H(2p) + H(2p) + O$ [31]. In the case of molecular emission, total fluorescence intensity pertaining to one electronic transition is often spread in several vibrational and rotational bands and can cover wavelength ranges of several tens of nanometers, which also increases the possibility of overlap with other emission systems. Indeed, using the present experimental set-up, we failed to observe photon-photon coincidences following photodissociation of the pyridine molecule into two excited molecular fragments, suspected to occur based on the similarities in their excitation functions [20], [22], [32]. Nevertheless, in complicated cases of many overlapping states, the photon–photon coincidence spectroscopy allows one to filter the populations of different states and thus it can be used for a proper identification of the lines and for studying the dynamics of Auger cascades.

Acknowledgments: We are grateful to the Elettra-Sincrotrone for providing beamtime no. 20145346. Staying of TJW in Elettra was in part financially supported under the CALIPSO contract provided through Elettra. TJW would like to thank professor M. Zubek for

expertise and insight throughout the project and beneficial discussions. We thank R. Richter for the possibility to use his Igor procedures in the data analysis. We are grateful to the staff of the Synchrotron Trieste for assistance, and particularly to Mr. G. Bortoletto of the Users' mechanical workshop.

CONFLICTS OF INTEREST

The authors declare that there is no conflict of interest regarding the publication of this article.

References

[1] N.M. Kabachnik , S. Fritzsche, A.N.Grum-Grzhimailo, M. Meyer, K. Ueda, Coherence and correlations in photoinduced Auger and fluorescence cascades in atoms, Phys. Rep. 451 (2007) 155 https://doi.org/10.1016/j.physrep.2007.07.005

[2] H. Aksela, S. Aksela, N. M. Kabachnik, in VUV and Soft X-Ray Photoionization, ed. Becker U and Shirley D.A., Plenum Press, New York and London (1996) p. 401

[3] M. Nakamura, M. Sasanuma, S. Sato, M. Watanabe, H. Yamashita, Y. Iguchi, A. Ejiri, S. Nakai, S. Yamaguchi, T. Sagawa, Y. Nakai, T. Oshio, Absorption Structure Near the $L_{II,III}$ Edge of Argon Gas, Phys. Rev. Lett. 21 (1968) 1303 https://doi.org/10.1103/PhysRevLett.21.1303

[4] G.C. King, M. Tronc, F.H. Read, R.C. Bradford, An investigation of the structure near the $L_{2,3}$ edges of argon, the $M_{4,5}$ edges of krypton and the $N_{4,5}$ edges of xenon, using electron impact with high resolution, J. Phys. B 10 (1977) 2479 https://doi.org/10.1088/0022-3700/10/12/026

[5] J.A.R. Samson, W.C. Stolte, Z.X. He, J.N. Cutler, D. Hansen, Postcollision interactions in the Auger decay of the Ar L shell, Phys. Rev. A 54 (1996) 2099 https://doi.org/10.1103/PhysRevA.54.2099

[6] J.A. de Gouw, J. van Eck, A.C. Peters, J. van der Weg, H.G.M. Heideman, Resonant Auger spectra of the $2p^{-1}$ nl states of argon, J. Phys. B 28 (1995) 2127 https://doi.org/10.1088/0953-4075/28/11/012

[7] J. Mursu, H. Aksela, O.-P. Sairanen, A. Kivimäki, E. Nõmmiste, A. Ausmees, S. Svensson, S. Aksela, Decay of the $2p^5 4s$, $2p^5 3d$ and $2p^5 4d$ states of Ar studied by utilizing the Auger resonant Raman effect, J. Phys. B 29 (1996) 4387 https://doi.org/10.1088/0953-4075/29/19/012

[8] S. Osmekhin, S. Fritzsche, A.N. Grum-Grzhimailo, M. Huttula, H. Aksela, S. Aksela, Angle-resolved study of the Ar $2p^{-1}_{1/2}3d$ resonant Auger decay, J. Phys. B 41 (2008) 145003 https://doi.org/10.1088/0953-4075/41/14/145003

[9] P. Lablanquie, S. Sheinerman, F. Penent, T. Aoto, Y. Hikosaka, K. Ito, Dynamics of double photoionization near the Ar 2*p* threshold investigated by threshold electron–Auger electron coincidence spectroscopy, J. Phys. B 38 (2005) L9 https://doi.org/10.1088/0953-4075/38/1/L02

[10] Y. Hikosaka, P. Lablanquie, F. Penent, P. Selles, E. Shigemasa, K. Ito, Resonant multiple Auger decay after the $2p^{-1}_{3/2}$ 4*s* excitation in Ar studied with a multielectron coincidence method, Phys. Rev. A 89 (2014) 023410 https://doi.org/10.1103/PhysRevA.89.023410

[11] E. Rühl, C. Heinzel, H.-W. Jochims, Fluorescence of Ar(2*p*)-excited argon clusters, Chem. Phys. Lett. 211 (1993) 403 https://doi.org/10.1016/0009-2614(93)87081-D

[12] J.A.R. Samson, Y. Lu, W.C. Stolte, Aspects of postcollision interactions near the Ar L shell, Phys. Rev. A **56** (1997) R2530 https://doi.org/10.1103/PhysRevA.56.R2530

[13] R. Flesch, H.-W. Jochims, J. Plenge, E. Rühl, Ultraviolet-visible fluorescence of 2*p*-excited argon, Phys. Rev. A 61 (2000) 062504 https://doi.org/10.1103/PhysRevA.61.062504

[14] M. Meyer, A. Marquette, A. Grum-Grzhimailo, R. Flesch, E. Rühl, Alignment of Ar^+ ions produced after resonant Auger decay of Ar* $2p^5 3d$ resonances, Surf. Rev. Lett 9 (2002) 141 https://doi.org/10.1142/S0218625X02002063

[15] T. Gejo, M. Iseda, T. Tamura, K. Honma, J.R. Harries, Y. Tamenori, Investigation of the 2p ionization threshold region of Ar clusters by observation of the fluorescence lifetime, J. Electron Spectrsc. Relat. Phenom. 155, (2007) 119 https://doi.org/10.1016/j.elspec.2006.11.011

[16] T. Gejo, T. Ikegami, K. Honma, J.R. Harries, Y. Tamenori, Fluorescence decay processes following resonant 2p photoexcitation of Ar atoms and clusters studied using a time-resolved fluorescence and photoion coincidence technique, J. Phys. B: At. Mol. Opt. Phys. 46 (2013) 075102 https://doi.org/10.1088/0953-4075/46/7/075102

[17] J.A.R. Samson, Y. Chung, E.-M. Lee, Ar 3s, 3p satellite lines studied by fluorescence spectroscopy, Phys. Lett. A 127 (1988) 171 https://doi.org/10.1016/0375-9601(88)90095-3

[18] T. J. Wasowicz, A. Kivimäki, M. Dampc, M. Coreno, M. De Simone, M. Zubek, Photofragmentation of tetrahydrofuran molecules in the vacuum-ultraviolet region via superexcited states studied by fluorescence spectroscopy, Phys. Rev. A 83 (2011) 033411 https://doi.org/10.1103/PhysRevA.83.033411

[19] T. J. Wasowicz, A. Kivimäki, M. Coreno, M. Zubek, Superexcited states in the vacuum-ultraviolet photofragmentation of isoxazole molecules, J. Phys. B: At. Mol. Opt. Phys. 45 (2012) 205103 https://doi.org/10.1088/0953-4075/45/20/205103

[20] T. J. Wasowicz, A. Kivimäki, M. Coreno, M. Zubek, Formation of CN ($B^2\Sigma^+$) radicals in the vacuum-ultraviolet photodissociation of pyridine and pyrimidine molecules, J. Phys. B: At. Mol. Opt. Phys. 47 (2014) 055103 https://doi.org/10.1088/0953-4075/47/5/055103

[21] M. Zubek, T. J. Wasowicz, I. Dabkowska, A. Kivimäki, M. Coreno, Hydrogen migration in formation of NH($A^3\Pi$) radicals via superexcited states in photodissociation of isoxazole molecules, J. Chem. Phys. 141 (2014) 064301 https://doi.org/10.1063/1.4891808

[22] T. J. Wasowicz, I. Dabkowska, A. Kivimäki, M. Coreno, M. Zubek, Elimination and migration of hydrogen in the vacuum-ultraviolet photodissociation of pyridine molecules, J. Phys. B: At. Mol. Opt. Phys. 50 (2017) 015101 https://doi.org/10.1088/1361-6455/50/1/015101

[23] H. Pulkkinen, S. Aksela, O.-P. Sairanen, A. Hiltunen, H. Aksela, Correlation effects in the $L_{2,3}$- MM Auger transitions of Ar, J. Phys. B 29 (1996) 3033 https://doi.org/10.1088/0953-4075/29/14/016

[24] A. Kramida, Yu. Ralchenko, J. Reader and NIST ASD Team (2018). NIST Atomic Spectra Database (ver. 5.5.2), [Online]. Available: http://physics.nist.gov/asd [2018, January 9]. National Institute of Standards and Technology, Gaithersburg, MD.

[25] A. Hibbert, Calculation of Rates of 4*p*–4*d* Transitions in Ar II, Atoms 5 (2017) 8 https://doi.org/10.3390/atoms5010008

[26] M. T. Belmonte, S. Djurović, R. J. Peláez, J. A. Aparicio, S. Mar, Improved and expanded measurements of transition probabilities in UV Ar ii spectral lines, Mon. Not. R. Astron. Soc. 445 (2014) 3345-3351 https://doi.org/10.1093/mnras/stu2006

[27] E. G. Berezhko, N. M. Kabachnik, Theoretical study of inner-shell alignment of atoms in electron impact ionisation: angular distribution and polarisation of X-rays and Auger electrons, J. Phys. B: At. Mol. Phys. 10 (1977) 2467 https://doi.org/10.1088/0022-3700/10/12/025

[28] Ch. Ozga, Ph. Reiß, W. Kielich, S. Klumpp, A. Knie and A. Ehresmann, Fluorescence cascades after excitation of XeII $5p^4 6p$ satellite states by synchrotron radiation, J. Phys. B: At. Mol. Opt. Phys. 48 (2015) 015004 https://doi.org/10.1088/0953-4075/48/1/015004

[29] M. Meyer, A. Marquette, A. N. Grum-Grzhimailo, U. Kleiman, B. Lohmann, Polarization analysis of fluorescence probing the alignment of Xe^+ ions in the resonant Auger decay of the Xe* $4d_{5/2}^{-1}$ photoexcited state, Phys. Rev. A 64, 022703 (2001) https://doi.org/10.1103/PhysRevA.64.022703

[30] B. M. Lagutin, I. D. Petrov, Ph. V. Demekhin, V. L. Sukhorukov, F. Vollweiler, H. Liebel, A. Ehresmann, S. Lauer, H. Schmoranzer, O. Wilhelmi, B. Zimmermann, K-H. Schartner, Alignment of ions after autoionization decay of atomic resonances: I. The $4d^9_{5/2}6p_{3/2}(J = 1)$ resonance in Xe, J. Phys. B: At. Mol. Opt. Phys. **33** (2000) 1337–1356 https://doi.org/10.1088/0953-4075/33/7/304

[31] T. Odagiri, M. Nakano, T. Tanabe, Y. Kumagai, I.H. Suzuki, M. Kitajima, N. Kouchi, Three-body neutral dissociations of a multiply excited water molecule around the double ionization potential, J. Phys. B: At. Mol. Opt. Phys. 45 (2012) 215204 https://doi.org/10.1088/0953-4075/45/21/215204

[32] T. J. Wasowicz, A. Kivimäki, M. Coreno, M. Zubek, Hydrogen migration in photodissociation of the pyridine molecules, J. Phys.: Conf. Ser. 635 (2015) 112049 https://doi.org/10.1088/1742-6596/635/11/112049